Δ VLBI Spacecraft Tracking System Demonstration: Part I. Design and Planning

D. L. Brunn, R. A. Preston, S. C. Wu, H. L. Siegel, D. S. Brown
Tracking Systems and Applications Section

C. S. Christensen and D. E. Hilt
Navigation Systems Section

The current status of planned Δ VLBI Navigation demonstrations during Voyager Jupiter encounters is discussed. Error analysis indicates angular accuracies of 0.05 μrad are possible. Near real-time data transmission can be achieved with minimal station hardware and software modifications. A software correlator and phase tracking program, operating on the SFOF IBM 360, will be used for data processing. Data quality tests will begin on July 1978 and formal demonstrations will start on January 1979.

I. Introduction

This article is the first of a planned series which will describe the DSN development of an improved spacecraft navigation system utilizing Very Long Baseline Interferometry (VLBI) techniques. Each article is intended to provide an overview of the work accomplished for the reporting phase. Detailed analysis will be covered in separate articles. This report covers the Design and Planning phase of a planned Δ VLBI navigation demonstration using the Voyager spacecraft near Jupiter encounter. For background information the reader is referred to Ref. 1, which develops the basic theory of this navigation technique.

First it is worth while to discuss why we are developing this technique, how it relates to current DSN VLBI development efforts, and what the basic techniques are.

The main drivers may be summarized as follows:

(1) Increased efficiency of tracking station utilization for navigation

(2) Potentially more accurate estimates of right ascension α, declination δ, and their time derivatives than conventional doppler and range

(3) Lower processing costs

(4) Not limited by round-trip light times

Achievement of these desirable features appears to be well within current spacecraft and DSN technological capabilities. The need for increased operational efficiency and lower costs are well established facts. Preliminary studies have shown that

the increased measurement accuracy can provide significant mission enhancement for future projects such as Galileo.

Figure 1 shows the interrelationship of current VLBI technology applications and the development of same for spacecraft navigation purposes. Interferometric techniques have been used by radio astronomers for extra-galactic radio source (EGRS) position and structure measurements for a number of years. The DSN has been actively building a precision VLBI capability in order to better calibrate the network as an instrument for conventional radio metric navigation (Refs. 2-9).

When the interferometer is used to track essentially the downlink carrier, the data type obtained is called differential one-way doppler; when a broadband signal is supplied and tracked, the data type obtained is referred to as differential one-way ranging. When the spacecraft signal and a nearby (in angular measure) EGRS are alternately tracked, the data is referred to as Δ VLBI (the Δ in this case refers to the fact that the spacecraft and the EGRS are being differentially tracked). There are two fundamental types of Δ VLBI data: narrow-band and wide-band, again depending on the bandwidth being supplied (and used) by the spacecraft RF waveform. The distinguishing features of each technique are as follows.

A. Narrowband Δ VLBI

The observables are the spacecraft S- or X-band carrier signals and a nearby (<10 deg) radio source. A single baseline is used that has a large equatorial component. The signals must be observed throughout the common view period, since the geometric changes occurring due to the Earth's rotation are needed to separate the declination and right ascension components. The measurement accuracy is declination angle dependent and angular accuracy for $\delta > 20$ deg is < 0.05 μrad. Typical measurement times are four hours.

B. Differential One-Way Range (DOR)

The observables are spacecraft generated signals that have a spanned bandwidth in the order of 50 MHz. The differences in time of arrival are interferometrically measured over two baselines and the spacecraft angular position is determined from this information. The measurement accuracy is declination angle independent. Angular accuracies of 0.05 μrad are achievable with spanned bandwidths on the order of 50 MHz and sub-nanosecond clock synchronization. Measurement time is typically ten minutes per baseline.

C. Wideband Δ VLBI

This tracking technique alternately measures the wideband spacecraft signals and signals from a nearby EGRS. The measurements are made over two baselines and the spacecraft position with respect to the EGRS are determined. The measurement accuracy is declination angle independent. Angular accuracies of < 0.05 μrad are possible since there is a large degree of error source cancellation due to the differential nature of the measurement. A significant advantage is relaxation of the sub-nanosecond clock synchronization requirement as needed by DOR. Measurement time is typically twenty minutes per baseline.

The Voyager spacecraft does not produce the wide bandwidth signals needed for precision DOR or wideband Δ VLBI measurements. Restricted bandwidth measurements, using harmonics of the unmodulated 360-kHz telemetry subcarrier, are being attempted for engineering purposes. Narrowband Δ VLBI measurements are quite possible using the spacecraft S- or X-band carriers and the Goldstone/Canberra or Goldstone/Spain baselines. The following sections will describe the planning and design of such a demonstration to be performed during the Jupiter encounter phases of Voyagers 1 and 2. Information concerning trajectory and source positions, error allocation estimates, data requirements, data acquisition and processing system and the demonstration plan will be presented.

II. Narrowband Δ VLBI Demonstration Plan

The objective of the demonstration is to demonstrate the utility and viability of Δ VLBI as a deep space navigation data type. The plan for achieving the objective is to first determine the position of Jupiter with respect to an EGRS (OJ287) using Δ VLBI and conventional doppler and range from Voyager 1. Then, using this improved Jupiter ephemeris and Δ VLBI for Voyager 2, the encounter conditions of this spacecraft will be predicted at about 30 days before the encounter takes place (Fig. 2).

Δ VLBI for Voyager 1 will be taken pre- and post-encounter in order to determine the motion of the spacecraft with respect to OJ287 (vector B) (Fig. 14). The pre- and post-encounter conventional doppler and range will produce a very accurate determination of Voyager 1 with respect to Jupiter (vector A). Combining these will yield the motion of Jupiter with respect to OJ287 (vector C). Δ VLBI for Voyager 2 taken pre-encounter will then be used to determine the spacecraft motion with respect to OJ287 (vector D). The motion of Voyager 2 with respect to Jupiter (vector E) can then be predicted.

A. Data Acquisition Strategies

The data will first be used for system testing and data quality checks. Thus, from July 1978 to December 1978, one Δ VLBI pass per month will be sufficient for testing purposes.

During January 1979 to April 1979 eight passes of Δ VLBI will be taken from Voyager 1 and OJ287. Four of the passes will be pre-encounter and four post-encounter. If possible, these passes will be symmetrically spaced with respect to encounter, e.g., one 40 days before, one 40 days after, one 20 days before, one 20 days after, etc. Further, antenna availability permitting, at least one of the passes will be within 10 days of encounter.

The gathering of Δ VLBI from Voyager 2 will begin in May 1979 and end in June of 1979. Four passes taken on a once per week basis, will be used to predict the encounter of Voyager 2.

B. Data Differencing Strategies

Narrow-band Δ VLBI from 2 stations can be defined as:

$$Z(t) = \{\rho_2(t) - \rho_2(t_0) - [\rho_1(t) - \rho_1(t_0)]\}$$

$$- \{\rho_2^*(t) - \rho_2^*(t_0) - [\rho_1^*(t) - \rho_1^*(t_0)]\} \qquad (1)$$

where the

$\rho_i(t)$ = range to station i at time t

'*' = indicates range from the EGRS

t_0 = beginning of pass

This data type is then seen to be the difference of accumulated phase of the spacecraft, and EGRS, from two stations. The expression in the first set of brackets is the difference of conventional doppler. In this mode, the two stations alternate in both receiving from the spacecraft and then the quasar.

If four stations are used, then two receive only from the spacecraft, one at each end of the baseline, and the other two receive only from the EGRS.

In order to nearly cancel the transmission media effects on the received signals, it is necessary to choose different times for differencing the spacecraft and EGRS data. In general, then, Δ VLBI will be defined as

$$Z(t, t^1) = \{[\rho_2(t) - \rho_2(t_0)] - [\rho_1(t) - \rho_1(t_0)]\}$$

$$- \{[\rho_i^*(t^1) - \rho_i^*(t_0^1)] - [\rho_j^*(t^1) - \rho_j^*(t_0^1)]\} \qquad (2)$$

where

$i = 2, j = 1$ for 2 station measurements

$i = 3, j = 4$ for 4 station measurements

t, t^1 are chosen so that the residual transmission media effects on $Z(t,t^1)$ are a minimum, as discussed in Section IV.

C. Demonstration Conduct

The demonstration will be conducted on a non-interference basis with Voyager operations using the near real-time system described in Section VII.

The processing of the data will be in parallel with Voyager operations. The navigation processing of Δ VLBI will be done on the Univac 1108 with a demonstration version of the Orbit Determination Program (ODP).

For Voyager 1, the demonstration will use the conventional radio-determined spacecraft trajectory as *a priori* for improvements to be obtained using Δ VLBI. The ephemeris of Jupiter will be the same as that used by the Navigation Team. After the encounter of Voyager 1, the Navigation Team trajectory and Δ VLBI will be processed to improve the ephemeris of Jupiter relative to OJ287. All spacecraft acceleration histories, timing and polar motion parameters, and astrodynamic constants will be supplied by the Navigation Team.

For Voyager 2 the spacecraft event histories will be supplied by the Navigation Team. The improved ephemeris of Jupiter relative to OJ287 and Δ VLBI data will be the only inputs different from those used by the Navigation Team.

III. Extra Galactic Radio Source Positions

Since the magnitudes of most Δ VLBI systematic error sources are proportional to the angular separation of the spacecraft and the EGRS, it is important to have a high spatial density of radio sources along the spacecraft flight path. Over the last few years, the DSN VLBI development effort has found a number of VLBI sources near the path of the ecliptic plane in the sky. Due to the upcoming Δ VLBI demonstration, increased emphasis has recently been placed on identifying sources along the appropriate portions of the Voyager trajectories.

For a celestial radio source to be useful for VLBI, it should possess components that are no larger in angular extent than the fringe spacing of the interferometer. The interferometer

fringe spacing is equal to the observed wavelength divided by the length of the component of the baseline that is perpendicular to the source direction. So for S-band observations with antennas separated by intercontinental distances, the interferometer sees only the radio flux coming from source components which are smaller than about 10 or 20 nanoradians in extent. Only a small fraction of celestial radio sources are that small. The search for VLBI sources has proceeded by examining with VLBI only those celestial radio sources whose intrinsic properties (e.g., spectra, variability) indicate that compact components might be present.

Figure 3 shows the present status of the search for VLBI sources in the region of the ecliptic in which the Voyager demonstration will occur. Also plotted are the nominal trajectories for the two Voyager spacecraft (JST and JSX). S-band VLBI source strengths, or correlated flux densities, are shown in parentheses next to each source (1 jansky = 10^{-26} W/m^2-Hz). X-band searches have been performed, but not yet analyzed. This figure shows that at least 25 VLBI sources with flux densities greater than 0.1 Jansky are potentially available for use in the Voyager demonstration. If the lower limit on source strength is raised to 0.4 Jansky, then the number of possible sources falls to under 10. It should be noted that the spatial distribution of these sources is rather uneven. Future searches for VLBI sources will attempt to fill in some of these gaps.

The brightest VLBI source close to the Voyager flight paths is OJ287. A time history of correlated flux density for OJ287 over the last three years using Goldstone-Australia and Goldstone-Spain baselines is shown in Fig. 4. More than a factor of two decrease in S-band source strength is apparent during that time period. A variation in VLBI source strength by a factor of two or more on a time scale of months or years is a very common property of VLBI sources. In addition, equally large variations in source strength may occur during a few hour period of observation. These short-term variations are not due to variations in the source itself, but are due to the fact that the interferometer fringe pattern changes throughout an observing period of a few hours and hence allows the interferometer to see different size elements of the source at different times. This effect also allows the source strength to vary from baseline to baseline. In the case of OJ287, the source is unusually compact, so that variations in strength caused by baseline orientation or length are not significant.

Due to both the baseline induced and intrinsic variations in source strength, the quoted strengths of the VLBI sources in Fig. 3 should be assumed to be only approximations. Any set of sources that might eventually be utilized for Δ VLBI navigation should be regularly monitored for both types of source strength variation on the same baselines that will be utilized for Δ VLBI navigation measurements. In addition, Fig. 4 shows that the X-band strength of OJ287 differs from the S-band strength. The difference is due not only to different intrinsic source strengths at X- and S-band, but also to the different size fringe spacing at the two frequencies. Hence, the source monitoring program should be carried out at the same frequency(s) which will be utilized during Δ VLBI navigation measurements.

Further VLBI measurements of the ecliptic VLBI sources will also be required in order to perform accurate determinations of their relative positions. The accurate positional information is important if accurate navigation from EGRS to EGRS or EGRS to planet is to be performed. Even with poorer knowledge of source positions, precision measurement of spacecraft-EGRS angular rate is still a valuable navigation tool.

IV. Estimate of Error Sources

This section provides estimates of the error sources affecting narrow-band Δ VLBI performance. Since Δ VLBI measures only the relative angular position between the spacecraft and a nearby EGRS, the spacecraft angular position accuracy with respect to a planet is the RSS of the measurement accuracy and the accuracy of the planetary ephemeris. In the following, each error source to which the Δ VLBI measurement is sensitive is studied separately. Numerical estimates are calculated for the geometry during Jupiter encounters of the two Voyager spacecraft. The RSS error is then compared to the 0.05 μrad error budget. Planetary ephemeris errors will be considered separately.

A. Baseline Error

The information content of a narrowband Δ VLBI can be represented by the equation:

$$\Delta\rho = -B_e \cos\delta_* [\cos(\alpha_B - \alpha_*) - \cos(\alpha_{B,i} - \alpha_*)]\ \Delta\alpha$$

$$-B_e \sin\delta_* [\sin(\alpha_B - \alpha_*) - \sin(\alpha_{B,i} - \alpha_*)]\ \Delta\delta \quad (3)$$

where

$\Delta\rho$ = accumulated differential range delay

B_e = equatorial component of the baseline

α_*, δ_* = right ascension and declination of the EGRS

$\Delta\alpha, \Delta\delta$ = separations in right ascension and in declination of the spacecraft from the EGRS

α_B = right ascension of the baseline center, a function of time

$\alpha_{B,i}$ = initial value of α_B

The separation ($\Delta\alpha$, $\Delta\delta$) can be determined from the diurnal variation of the above equation. For this purpose Eq. (3) is rearranged into the following form:

$$\Delta\rho = A[\cos(\omega_e t + \alpha_\odot + \lambda_B - \alpha_* - \Psi) - \cos(\omega_e t_0 + \alpha_\odot + \lambda_B - \alpha_* - \Psi)] \quad (4)$$

where

$$A = B_e[\cos^2\delta_*(\Delta\alpha)^2 + \sin^2\delta_*(\Delta\delta)^2]^{1/2} \quad (5)$$

$$\Psi = \tan^{-1}\frac{\Delta\delta\tan\delta_*}{\Delta\alpha}$$

ω_e = 73 μrad/sec = the Earth's spin rate

$\alpha_\odot$ = right ascension of the Sun

λ_B = longitude of the center of baseline

It is observed that an error in B_e will result in a change in the amplitude A of the diurnal variation which in turn will result in $\Delta\alpha$ and $\Delta\delta$ estimation error; an error in λ_B will result in the same amount of error in Ψ and in turn will result in $\Delta\alpha$ and $\Delta\delta$ estimation error. The sensitivity of $\Delta\alpha$ and $\Delta\delta$ to the error in B_e and λ_B can be estimated by constructing the following matrix using Eqs. (4) and (5):

$$\begin{bmatrix} \frac{\partial B_e}{\partial(\Delta\alpha)} & \frac{\partial B_e}{\partial(\Delta\delta)} \\ \frac{\partial\Psi}{\partial(\Delta\alpha)} & \frac{\partial\Psi}{\partial(\Delta\delta)} \end{bmatrix} = \frac{1}{(\Delta\alpha)^2\cos^2\delta_* + (\Delta\delta)^2\sin^2\delta_*} \begin{bmatrix} -(\Delta\alpha)B_e\cos^2\delta_* & -(\Delta\delta)B_e\sin^2\delta_* \\ -(\Delta\delta)\sin\delta_*\cos\delta_* & (\Delta\alpha)\sin\delta_*\cos\delta_* \end{bmatrix} \quad (6)$$

The inversion of this matrix yields the following simple result

$$\begin{bmatrix} \epsilon_{\Delta\alpha} \\ \epsilon_{\Delta\delta} \end{bmatrix} = \begin{bmatrix} \frac{\partial B_e}{\partial(\Delta\alpha)} & \frac{\partial B_e}{\partial(\Delta\delta)} \\ \frac{\partial\Psi}{\partial(\Delta\alpha)} & \frac{\partial\Psi}{\partial(\Delta\delta)} \end{bmatrix}^{-1} \begin{bmatrix} \epsilon_{B_e} \\ \epsilon_\Psi \end{bmatrix} \quad (7)$$

$$= \begin{bmatrix} -\Delta\alpha/B_e & -\Delta\delta\tan\delta_* \\ -\Delta\delta/B_e & \Delta\alpha\cot\delta_* \end{bmatrix} \begin{bmatrix} \epsilon_{B_e} \\ \epsilon_{\lambda_B} \end{bmatrix}$$

The angular separation error of interest is $(\epsilon^2_{\Delta\alpha}\cos^2\delta_* + \epsilon^2_{\Delta\delta})^{1/2}$. Note that the zero-$\delta$ singularity appears only with $\epsilon_{\Delta\delta}$ due to the error in λ_B.

The error components containing $\Delta\alpha$ can be eliminated by taking the spacecraft quasar observations at times separated by $\Delta t = \Delta\alpha/\omega_e$. For instance, if $\Delta\alpha = \alpha_{S/C} - \alpha_* = 2$ deg, the baseline error will be eliminated by taking spacecraft observations 8 minutes after corresponding EGRS observations. This is true since the $\Delta\rho$ so constructed is equivalent to that for $\Delta\alpha = 0$. The time offsetting may introduce another error due to *nonlinear* clock drift. This will be discussed later.

B. Polar Motion Error

It has been shown (Ref. 2) that an error in X- or Y-component of polar motion will result in an error in VLBI measurement z/a times that due to an error in x- or y-component of the baseline where z is the z-component of the baseline and a is the Earth's radius. This relationship is still valid in the case of ΔVLBI. For a Goldstone/Canberra baseline $z \doteq a$ and the error in X and Y is of the same order of magnitude as that in x- and y-components of the baseline.

Hence Δ VLBI error due to polar motion can be estimated to be statistically equal to that due to baseline error.

C. UT1 Error

From Eq. (4) it can be seen that an error in time can be translated into an error in λ_B. Hence an error in UT1 of ϵ_t will result in an error in $\Delta\alpha$ and $\Delta\delta$ of

$$\begin{aligned} \epsilon_{\Delta\alpha} &= (\omega_e \, \Delta\delta \, \tan\delta_*) \, \epsilon_t \\ \epsilon_{\Delta\delta} &= -(\omega_e \, \Delta\alpha \cot\delta_*) \, \epsilon_t \end{aligned} \tag{8}$$

Current capability indicates $\epsilon_t \doteqdot 2$ mS. The projected capability during Voyager encounter is $\epsilon_t \doteqdot 1$ mS.

D. System Noise

In Δ VLBI measurement the EGRS, being a distant radio source, has a very low signal level. On the other hand the receiver has an inherent noise that is orders of magnitude higher than the EGRS signal at any frequency within the receiver passband. However, the EGRS signals received at the two ends of the baseline are highly correlated, while the system noises are not. Doubling the bandwidth increases the signal level by a factor of 2 while the noise is increased only by a factor of $\sqrt{2}$. The signal to noise ratio of the correlation signal is

$$SNR = \frac{2}{\pi} \frac{10^{-26}}{2K} S \frac{\pi}{4} d_1 d_2 \sqrt{\frac{e_1 e_2 BT}{T_{S,1} T_{S,2}}} \tag{9}$$

where

K = Boltzmann's constant (1.38×10^{-23})W-s/deg.

S = total observed flux density of source over baseline of interest (Jansky = 10^{-26} W/m^2 - Hz)

d_1, d_2 = physical antenna diameter (m) at DSS_1, DSS_2

e_1, e_2 = antenna aperture efficiency at DSS_1, DSS_2

B = VLBI receiver filter bandwidth, Hz

T = integration time(s) per fringe phase point

T_{s_1}, T_{s_2} = total system noise temperature (K) at DSS_1, DSS_2

As will be shown in Section IV, spacecraft signals can each be correlated with a local model (essentially noise-free) and the resulting SNR is much higher than that of EGRS signals. Hence it is the EGRS SNR that is of concern. The effect of SNR on $\Delta\rho$ in Eq. (3) is

$$\begin{aligned} \epsilon_{\text{phase}} &= \frac{1}{\text{SNR}} \\ \therefore \; \epsilon_{\Delta\rho} &= \left(\frac{1}{\text{SNR}}\right) \frac{c}{2\pi f} \end{aligned} \tag{10}$$

where

c = speed of light

f = effective bandpass center

The minimum SNR for which EGRS signals can be phase tracked from VLBI measurements is about 5–10. This corresponds to ~ 0.42 cm error in $\Delta\rho$ at S-band. It is now desired to have a means to estimate the sensitivity of the determination of the angular separation to the system noise. Precise estimation requires an integral over the pass (~ 4 hours) which will not provide much insight. A U-V plane approach which is first used by Melbourne and Curkendall for Navigation (Ref. 1) and which is normally good to within a factor of 2, is adopted here. Let:

$$\begin{aligned} U &= \frac{1}{\cos\delta_*} \frac{\partial(\Delta\rho)}{\partial(\Delta\alpha)} \\ V &= \frac{\partial(\Delta\rho)}{\partial(\Delta\delta)} \end{aligned} \tag{11}$$

When Eq. (3) is substituted into Eq. (11) we see that the (U,V) vector will trace out an ellipse as the earth spins (i.e., α_B increases):

$$\left[\frac{U - B_e \cos(\alpha_{B,i} - \alpha_*)}{B_e}\right]^2 + \left[\frac{V - B_e \sin\delta_* \sin(\alpha_{B,i} - \alpha_*)}{B_e \sin\delta_*}\right]^2 = 1 \tag{12}$$

An example of such ellipse is shown in Fig. 5. The information content of angular separation in the direction of a (U,V) vector for a single instantaneous measurement is proportional to the length of the vector. The information content in the orthogonal direction is proportional to the component in this direction of the change in the (U,V) vector. For fringe-phase Δ VLBI, the change in the (U,V) vector is always in the same direction as the (U,V) vector itself near the beginning of the pass and little information in the orthogonal direction is

available. To acquire this information a long pass is required. For a long pass of Δ VLBI measurement, the information can be shown to be inversely proportional to:

$$\sigma_T^2 \doteqdot \sigma_{\Delta\rho}^2 \left[\frac{2}{S_r^2} + \frac{2}{S_\perp^2}\right] \quad (N/3) \tag{13}$$

where

$\sigma_{\Delta\rho}^2$ = the variance of the measured $\Delta\rho$

S_r = maximum vector length $(\mathbf{U}^2 + \mathbf{V}^2)^{1/2}$ over the pass

$S_\perp$ = maximum accumulated change of the vector **(U,V)** in the direction orthogonal to the **(U,V)** vector with maximum length

N = number of samples over the pass

3 = minimum number of samples required to acquire information in two orthogonal directions

For $\delta_* = 20$ deg and Goldstone/Canberra baseline, a four-hour pass results in $S_r \doteqdot 3200$ km, $S_\perp \doteqdot 800$ km. With $N = 240$ (1 sample/minute) and $\Delta\rho = 0.42$ cm, the error in the estimated angular separation is $\sigma_T \doteqdot 1$ nrad.

E. Transmission Media Error

The effect of transmission media on Δ VLBI angular separation measurement can be considered to be that of a frequency noise[1]. It differs from the usual system noise (a phase noise) in that the effect may build up over the pass, resulting in a non-zero accumulated error. For instance a 1 mm/s frequency noise, sampled every 1 minute over 4 hours, will result in an accumulated error of $(0.1 \times 60) \times \sqrt{4 \times 60} \doteqdot$ 93 cm. Hence an accumulated media error of 93 cm can be approximately represented by a frequency noise of 1 mm/sec. With this frequency-noise concept, the effect on Δ VLBI angular separation measurements can be easily estimated by an information ellipse similar to subsection (D) above.

The **(U,V)** vector is now defined as

$$\mathbf{U} = \frac{1}{\cos\delta_*}\frac{\partial(\Delta\dot{\rho})}{\partial(\Delta\alpha)}$$

$$\mathbf{V} = \frac{\partial(\Delta\dot{\rho})}{\partial(\Delta\delta)} \tag{14}$$

where the dots denote time derivatives. When Eq. (3) is substituted into Eq. (14) the following information ellipse is constructed:

$$\left(\frac{U}{\omega_e B_e}\right)^2 + \left(\frac{V}{\omega_e B_e \sin\delta_*}\right)^2 = 1 \tag{15}$$

This is shown in Fig. 6.

The information is inversely proportional to

$$\sigma_T^2 \doteqdot \sigma_{\Delta\rho}^2 \left[\frac{2}{S_r^2} + \frac{2}{S_\perp^2}\right] \Big/ (N/2) \tag{16}$$

with S_r, $S_\perp$ and N as defined in Section 4 above; the minimum number of samples is 2 in this case. As an example, for the same geometry as in Section 4 we obtain $S_r \doteqdot 420$ m/sec, $S_\perp \doteqdot 220$ m/sec. Hence the error in the estimated angular separation for 1 mm/sec frequency noise is 0.66 μrad. In other words, a 1-cm accumulated media error will result in $660/93 \doteqdot 7$ nrad error in angular separation estimation. To calculate the angular separation errors the accumulated errors in cm are multiplied by the sensitivity, 7 nrad/cm, estimated by the information ellipse. Hence, the accumulated media error must be limited to not more than a few centimeters. The accumulated media error is estimated separately for troposphere, ionosphere and solar plasma in the following.

1. Troposphere. The accumulated tropospheric effect is mainly due to the difference in elevation angles between the four ray paths. Zenith tropospheric effects can be calibrated by a surface model (Ref. 10) or a seasonal model (Ref. 11) to better than 6 cm at each DSS. Hence the residual effect at *either* DSS is

$$\epsilon = 6 \left| \frac{1}{\sin\gamma_{S/C}} - \frac{1}{\sin\gamma_*} \right| \text{ cm} \tag{17}$$

where $\gamma_{S/C}$ and γ_* are the elevation angles of the ray paths looking at the spacecraft and EGRS, respectively. The total effect is the RSS of the *accumulated* residual effects at the two DSS.

When the angular separation is in right ascension only, $\gamma_{S/C}$ and γ_* can be made equal by time offsetting as in the case of $\Delta\alpha$ component of baseline error. When the separation is in declination only a study shows that the difference of the two terms in Eq. (17) can be made nearly constant over the pass, also by time offsetting. The RSS accumulated residual effect

[1] This concept is suggested by J. K. Miller of the Navigation Systems Section.

can be reduced by up to two orders of magnitude. The optimum time offset with separation in both $\Delta\alpha$ and $\Delta\delta$ is

$$\Delta t = 4\ \Delta\alpha + 2.8\ \Delta\delta \text{ minutes} \tag{18}$$

where $\Delta\alpha$ and $\Delta\delta$ are in degrees. Of course, with such time offset the $\Delta\alpha$ component of the baseline error will not be completely eliminated. For JST Voyager encounter ($\Delta\alpha$ = -11.8 deg, $\Delta\delta$ = 0.7 deg) the residual accumulated effect is estimated to be reduced from 30 cm (Δt = 0) to 0.2 cm (Δt = 45.2 min). For JSX Jupiter encounter ($\Delta\alpha$ = 2.2 deg, $\Delta\delta$ = -2.5 deg) it is reduced from 0.6 cm (Δt = 0) to 0.4 cm (Δt = 1.8 min). That the improvement is marginal is due to the already small effect with Δt = 0, a result of near ideal separation ($\Delta\alpha \doteqdot -0.7\ \Delta\delta$) for which no time offset is needed. The 45-minute time offset for JST encounter may introduce another error due to the imperfect correlation between the measurements separated by such time offset. This is estimated to be ~ 1 cm in accumulated effect. The total tropospheric effect for JST is thus ~ 1 cm. For JSX encounter, the time offset is small and such imperfect correlation is negligible.

2. Ionosphere. The accumulated ionospheric effect is mainly due to the difference in the product of the elevation-angle factor $g(\gamma)$ and the solar-zenith-angle factor $f(X)$ where

$$g(\gamma) = \left\{ \left[(R_e + h_2)^2 - R_e^2 \cos^2\gamma\right]^{1/2} - \left[(R_e + h_1)^2 - R_e^2 \cos^2\gamma\right]^{1/2} \right\} \Big/ (h_2 - h_1) \tag{19}$$

with R_e = 6370 km, h_1 = 215 km and h_2 = 454 km, and where

$$f(X) = \begin{cases} 0.2 + 0.8 \cos^{2/3} X\,, & |X| < 90 \text{ deg} \\ 0.2\,, & |X| > 90 \text{ deg} \end{cases} \tag{20}$$

with X being the solar-zenith angle.

With time offsetting for the minimization of the tropospheric effect the $g(\gamma)$ effect of the ionosphere is also reduced to a negligible amount. However the $f(X)$ effect will be increased since the difference in X will be increased by time offsetting. The proper time offset is a compromise between minimizing these effects. For JST Voyager encounter the Sun-Earth probe angle is (SEP $\doteqdot$ 140 deg) so that the overlapped tracking will be during local night ($|X| > 90$ deg) at both DSS and the $f(X)$ effect is minimal. Hence one can use the full time offset which minimizes the tropospheric error. The estimated accumulated error, assuming a 20-cm calibration error[2] at γ = 90 deg and X = 0, is ~ 0.2 cm. For JSX Jupiter encounter, the small time offset (Δt = 1.8 min) which minimizes the tropospheric effect will increase $f(X)$ effect of the ionosphere only slightly and still can be used. The estimated accumulated error (SEP $\doteqdot$ 27 deg) is ~ 1.5 cm.

In actual calibration of the ionospheric effect, the geomagnetic-latitude adjustment has to be made to minimize the north-south horizontal gradient effect.

3. Solar plasma. The solar plasma effect on VLBI can be estimated by (Ref. 12)

$$\epsilon = 0.039 \left[10 \sin(\text{SEP})\right]^{-1.3} \left(\frac{\tau}{10}\right) 0.75 \tag{21}$$

where τ is the time for the solar wind to travel across the distance between the two ray paths. Assuming a solar wind velocity of 400 km/sec perpendicular to the two ray paths, the τ will vary in the range $15 < \tau < 26$ sec. For Δ VLBI, the separation between the two ray paths from a DSS looking at the spacecraft and EGRS, even at 1 deg separation, is 2 orders of magnitude greater than that between the two ray paths at different DSS but looking at the same source, spacecraft or EGRS. Hence, Eq. (19) is used to estimate the residual effect of VLBI (two ray paths looking at the same sources); the accumulated residual effect for Δ VLBI will be $\sqrt{2}$ times as large since the two effects for the two VLBI measurements can be considered to be uncorrelated. It should be pointed out that the time offsetting between the spacecraft and EGRS measurements discussed earlier will not affect the solar plasma error since we do not assume any cancellation between the spacecraft and EGRS measurements.

For JST Jupiter encounter, SEP $\doteqdot$ 140 deg. Since Eq. (21) is applicable to SEP $\leqslant$ 90 deg, the estimate will be conservative if SEP = 90 deg is used for any SEP > 90 deg. With this assumption we get $\epsilon < 0.4$ cm. For Δ VLBI the residual accumulated effect will be $0.4\sqrt{2} \doteqdot 0.6$ cm. A similar calculation for JSX Jupiter encounter yields a residual accumulated effect of 1.6 cm.

4. Clock error. One of the features of Δ VLBI is the complete cancellation of clock drift between the two DSS if simultaneous spacecraft and EGRS measurements are taken and differenced. With time offset between the two types of measurement (to reduce error in baseline, polar motion, UT1 and tropospheric effect) an error due to clock drift is

[2]Using on-site Faraday rotation measurement from ATS Satellite.

introduced. Clock bias and linear phase drift has no effect on Δ VLBI; the corrupting effect is the second-order clock drift (linear frequency drift). Let the frequency stability be $\Delta f/f$ over the time T of the pass, the accumulated error in Δ VLBI with a time offset Δt can be shown to be

$$\epsilon_{\Delta\rho} = \frac{c}{2} \frac{(\Delta f/f)}{T} (\Delta t)(2T + \Delta t) \tag{22}$$

where c is the speed of light.

For JST Jupiter encounter Δt = 45.2 min, and for JSX Jupiter encounter Δt = 1.8 min. Assuming $\Delta f/f = 10^{-14}$ and $T = 4$ hours, the accumulated error will be 0.89 cm and 0.03 cm, respectively. The resulting angular separation error (at 7 nrad/cm) will be 6.2 nrad and 0.2 nrad, respectively. These errors are at least an order of magnitude lower than the other error sources which are reduced by introducing time offset.

This analysis does underscore, however, the importance of the hydrogen maser level of clock performance implicitly assumed by using 10^{-14} in the calculation. Degradation to 10^{-13} would in effect seriously compromise the system ability to minimize the effects of calibration errors and would force the use of only very small separation angles.

5. **EGRS position error.** This error is here defined as the error in pinpointing the "center" or the source. Most well-known EGRS sources are determined to within 10 nrad in angular position. For OJ287, which will be approached by the Voyager spacecraft near encounters, the angular position has been determined to within 3 nrad.

The estimated error sources for the two Voyager Jupiter encounters are summarized in Figs. 7 and 8. The projected accuracy for baselines and polar motion is 0.5 m in each component; for UT1 it is 1 mS. The RSS errors are well within the 0.5 μrad budget, especially for JST Jupiter encounter.

Instrumental errors of the system will presumably be removed by the use of phase calibrators. Estimation of the residual errors will be made when the calibrator performance and filters are studied.

V. Data Requirements

For the narrowband Δ VLBI spacecraft system demonstration, radio signals from a spacecraft and EGRS are alternately received at two DSS, infinitely clipped, sampled at a rate twice the VLBI receiver filter bandwidth, and digitally crosscorrelated to produce fringe phase. The narrowband Δ VLBI system requires fringe phase data points with a signal-to-noise ratio (SNR) of 5-10 or more for successful phase tracking. Additionally, several fringe phase data points are required every five minutes for phase connection.

Assuming the EGRS is a white noise source over the VLBI receiver filter bandwidth then the fringe phase SNR for the digital crosscorrelation of signals from DSS_1 and DSS_2 is given by Eq. (7). Let the radio source for the VLBI measurement be a spacecraft carrier signal. Assume the spacecraft is a spectral line radio source in the VLBI receiver filter bandwidth. The fringe phase SNR for the digital crosscorrelation of the signal from DSS_1 and DSS_2 is given by Eq. (9).

An alternate technique to direct crosscorrelation of spacecraft signals is local model crosscorrelation. For local model crosscorrelation, the spacecraft signal is crosscorrelated with a locally generated model of the spacecraft signal to determine their phase difference. The phase SNR for the digital local model crosscorrelation at DSS_1 is

$$SNR = 2\sqrt{\frac{P_{c_1} T}{\pi K T_{s_1}}} \tag{23}$$

The phase produced by local model crosscorrelation at DSS_1 is differenced with the phase at DSS_2 to produce fringe phase. Not only does local model crosscorrelation have a distinct SNR advantage over direct crosscorrelation, but only a digital representation of a phase and not an entire spacecraft signal needs to be transmitted from the DSS to JPL for real time processing.

The total minimal number of bits required from each station per fringe phase point is:

$$N = 2BT \tag{24}$$

Figure 9 is a plot of the expected S-band EGRS VLBI performance using OJ287 on the Goldstone – Canberra baseline for the narrowband Δ VLBI spacecraft tracking system demonstration. The performance for all possible VLBI DSS combinations on this baseline is shown. Integration time refers to the time period over which crosscorrelation is performed to produce one fringe phase data point at the sample rate of 80 kbits/s.

Table 1 is a summary of data requirements for the S-band narrowband Δ VLBI spacecraft tracking system demonstration.

VI. Data Acquisition

Figures 10, 11 and 12 depict the hardware configurations needed for the near real time Δ VLBI data acquisition system at DSS 14, DSS 13, and DSS 42/43 and 61/63. The data acquisition system allows near real-time demonstration of either two or four station narrowband Δ VLBI spacecraft tracking. Additionally, a backup MK II capability simultaneously exists.

Very little additional equipment is needed at the operational stations. Specifically, a power divider is added to the VLBI Bandwidth Synthesis (BWS) Assembly which splits the baseband signal into two paths: one to the IF converter and subsequent IVC recorder (MK II) and the other to the Occultation Data Assembly (ODA) via a 40-kHz low-pass filter. The ODA contains an A/D converter and a Modcomp computer with disk and tape drive. The low-pass filter bandwidth is set by the ODA data rate capability which is specified as 80 kbps maximum. The ODAs will be installed at each 64-m station by mid-1978 and the multiplexers have two spare input ports, one of which will be assigned for VLBI use. Data will be recorded and time tagged using either modified PV-78 ODA software or new software. The resultant tape is played back via the 56-kbps GCF WBDL to the NOCC at JPL using the Telemetry Processor Assembly (TPA). Minor software changes may be needed for the TPA Modcomp to perform this function.

Since DSS 13 does not have an ODA or WBDL, the 40-kHz analog signal out of the BWS assembly at DSS 13 will be digitized, time tagged, and transmitted by microwave to DSS 14 via GCF 10 for transmission to JPL.

VII. Data Processing

The current R&D VLBI system (MK II) is designed for platform parameter calibration and clock synchronization. The measurement technique involves observation of large numbers of radio sources and utilizes wide bandwidths (2 MHz) with corresponding high sample rate (4 Mb/s). Data is recorded on video tape and is shipped to JPL for processing on a special purpose hardware correlator located at CIT.

Use of this data acquisition and processing system for spacecraft navigation has several disadvantages, i.e., long delays due to logistics, large data volume and limited use of the correlator, which is also used for radio astronomy purposes. An operational version of this system is being implemented by the DSN and is scheduled to be operational by July 1979. Unfortunately this is too late for the Voyager Δ VLBI demonstrations; therefore, an alternative R&D design is being implemented which will allow near-real time data transmission (Section V) and processing. The salient features of this processing system are described in the following paragraphs.

Radio Source VLBI data processing can be conceived of as a data compression stage followed by a parameter estimation stage. In the data compression stage we input pairs of data samples taken simultaneously at two DSS. The model geometric delay and velocity difference at the two stations are removed by delaying one bit stream and digitally heterodyning one bit stream with the differential phase rate. Then the two streams are crosscorrelated and averaged. Finally the residual velocity difference (residual fringe frequency) is detected with a Fourier transform and the phase is tracked with a least-squares technique. When there are large time gaps in the observation sequence, it becomes necessary to resolve 2π phase ambiguities, i.e., to connect phase. The parameter estimation stage improves a priori values for source positions, station baselines, UT1, station clock offsets and polar motion. This program called "Phasor" currently runs on the CIT IBM 370 (Ref. 13).

Several modifications are required for processing Δ VLBI navigation data. These are:

(1) The system must return results in "near real time". That is, Δ VLBI spacecraft orbit solutions should be available on the order of a day. The Mark II turnaround is on the order of weeks due to tape shipment delays. DSN plans are to implement the correlator and phase tracking functions on the SFOF IBM 360 computers and to transmit data sampled at 500 kbits/s to JPL via the GCF wideband data lines. The previously described R&D near real-time configuration (Section V) is being implemented to provide data sampled at a reduced 80 kbit/s rate. A preliminary version of the IBM 360 correlator will be utilized to implement this system in July 1978. It should be noted that the capability to operate the conventional 4-megabit video recorder system concurrently will be maintained.

(2) The system must be able to model spacecraft motion for local correlation. The spacecraft models will provide a local model to correlate each station separately. The extragalactic radio source data will continue to be cross-correlated in the conventional manner.

(3) The system must be able to phase track spacecraft data. Since the spacecraft signals are very narrow-band, the correlated amplitude does not fall off rapidly in the time domain. Thus a special version of the phase tracking is being prepared which just fits phase residual in one lag channel only.

(4) The system must be able to solve for spacecraft orbits. The R&D system will accomplish this by preparing a

file of phase observables – called the Δ VLBI data file on an 1108 readable tape. Then a special program, the Δ VLBI processor, will prepare the data for processing on the standard Voyager ODP (orbit determination program).

An overall block diagram of the system is shown in Fig. 13. Data is received and recorded in the NOCC by the network log processor/real-time monitor. These tapes along with observation times, baseline parameters, Earth rotation rate, EGRS α & δ, and precalculated time delay and clock offset information are input to the IBM 360 software correlator which produces the fringe frequency correlation coefficients. The correlator operates in a cross-correlation mode when processing EGRS signals and a local model or cross-correlation mode when processing spacecraft signals. This step in the processing compresses the data by a factor of approximately 10^6.

Further processing of the data is accomplished in the PHASOR program, which performs a least-squares fit to the correlator output data producing a refined estimate of the fringe phase residuals plus the best estimate model. The ODP pre-processor connects the residual fringe phase, recovers the model to produce the estimated true fringe phase versus time and formats this data for input to the ODP. From this data the ODP generates the desired spacecraft position relative to the EGRS.

References

1. W. G. Melbourne and D. W. Curkendall, "Radio Metric Direction Finding: A New Approach to Deep Space Navigation", AAS/AIAA Astrodynamics Specialist Conference Paper presented at Jackson Hole, Wyoming, September 7-9, 1977.
2. J. G. Williams, "Very Long Baseline Interferometry and Its Sensitivity to Geophysical and Astronomical Effects", JPL Space Program Summary, 37-62 Vol. II, March 31, 1970, pp. 49-55.
3. Slade, M. A., Preston, R. A., Harris, A. W., Skjerve, L. J., Spitzmesser, D. J., "A1SEP – Quasar Differential VLBI", *The Moon*, 17, 133-147.
4. Thomas, J. B., "An Analysis of Long Baseline Radio Interferometry," in *The Deep Space Network Progress Report*, Technical Report 32-1526, Vol. VII, p. 37, Feb. 1972.
5. Thomas, J. B., "An Analysis of Long Baseline Radio Interferometry, Part II," in *The Deep Space Network Progress Report*, Technical Report 32-1526, Vol. VIII, p. 29, May 1972.
6. Thomas, J. B., "An Analysis of Long Baseline Radio Interferometry, Part III," in *The Deep Space Network Progress Report*, Technical Report 32-1526, Vol. XVI, p. 47, Aug. 15, 1973.
7. Goldstein, R., "Clock Calibration Via Quasar," SPS 37-48 Vol. II, p. 79, Nov. 1967.
8. Hurd, W. J., "Preliminary Demonstration of Clock Synchronization by Radio Interferometry," in *The Deep Space Network Progress Report* 42-37.
9. Hurd, W. J., "DSN Station Clock Synchronization by Maximum Likelihood VLBI", *The Deep Space Network Progress Report*, TR 32-1526, Vol. 10.
10. A. L. Berman, *The Prediction of Zenith Range Refraction From Surface Measurements of Meteorological Parameters*, TR 32-1602, July 15, 1976.
11. K. L. Thuleen and V. J. Ondrasik, "The Repetition of Seasonal Variations in the Tropospheric Zenith Range Effect", DSN Progress Report, TR 32-1526, Vol. VI, December 15, 1971, pp. 83-98.
12. P. S. Callahan, "An Analysis of Viking S-X Doppler Measurements of Solar Wind Columnar Content Fluctuations", DSN Progress Report PR 42-44, April 15, 1977.
13. Purcell, G., "A Procedure for Preliminary Reduction of Bandwidth Synthesis Data," in *The Deep Space Network Progress Report*, Technical Report, 42-33.

Table 1. Data requirements for the S-band narrowband Δ VLBI spacecraft tracking system demonstration

DSS combination	EGRS crosscorrelation		Spacecraft crosscorrelation		Spacecraft local model crosscorrelation	
	T	N	T	N	T	N
64 m – 64 m	1.61×10^{1}	1.3×10^{6}	1.82	1.5×10^{5}	3.37×10^{-2}	2.7×10^{3}
64 m – 26 m	1.64×10^{2}	1.3×10^{7}	1.82×10^{1}	1.5×10^{6}	3.38×10^{-1}	2.7×10^{4}
26 m – 26 m	1.67×10^{3}	1.3×10^{8}	1.83×10^{2}	1.5×10^{7}	3.38×10^{-1}	2.7×10^{4}

SNR = 10, B = 40 kHz
T = integration time in seconds per fringe phase point
N = number of bits per station per fringe phase point
OJ287 quasar radio source (0.8J correlated flux density for Goldstone — Canberra baseline)
Voyager spacecraft at JSX Jupiter encounter (64 m P_c = – 150.3 dBm, 26 m P_c = -158.5 dBm)

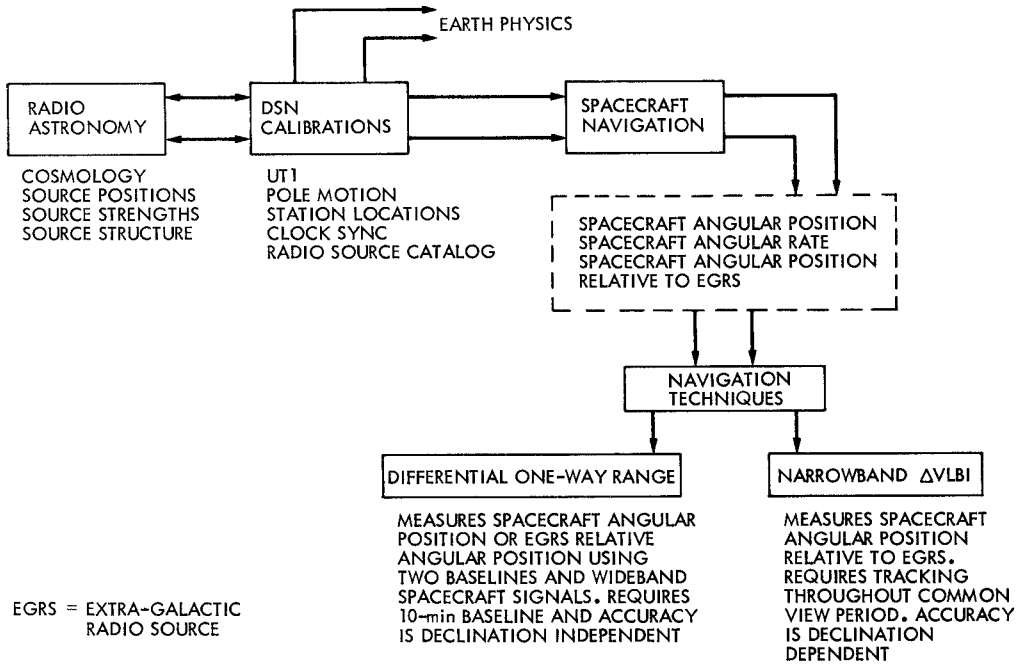

Fig. 1. Applications of very long baseline interferometry

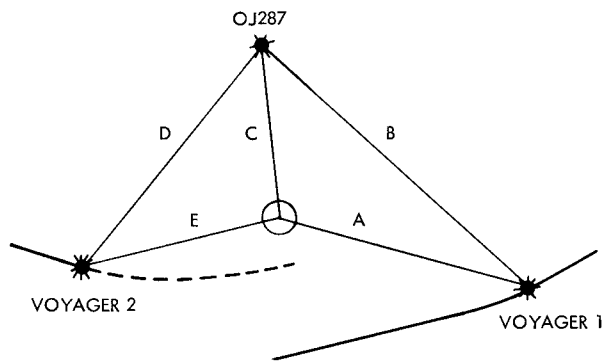

Fig. 2. Voyager 1/2 Jupiter encounter (plane of sky)

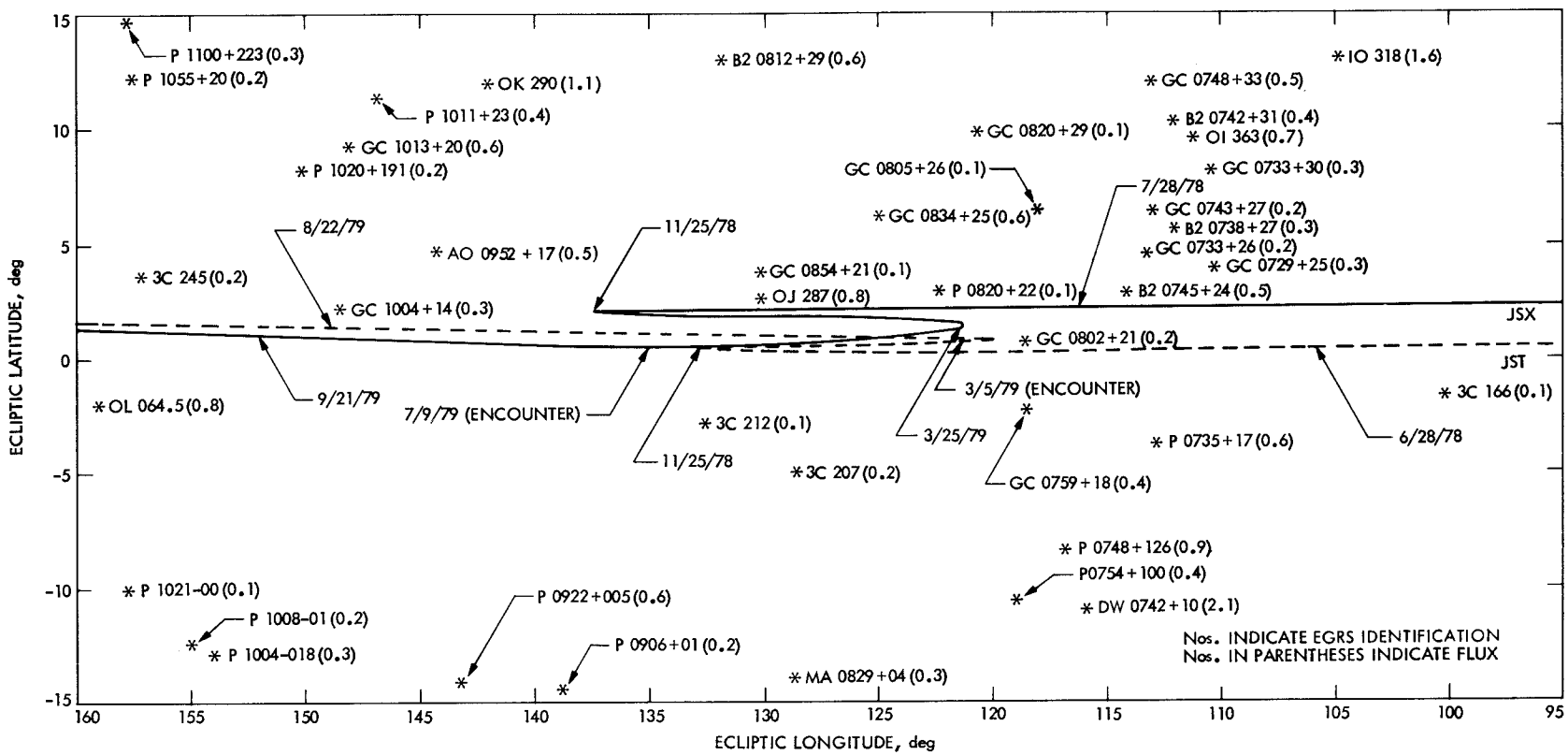

Fig. 3. Ecliptic VLBI source catalog for Voyager Δ VLBI demonstration

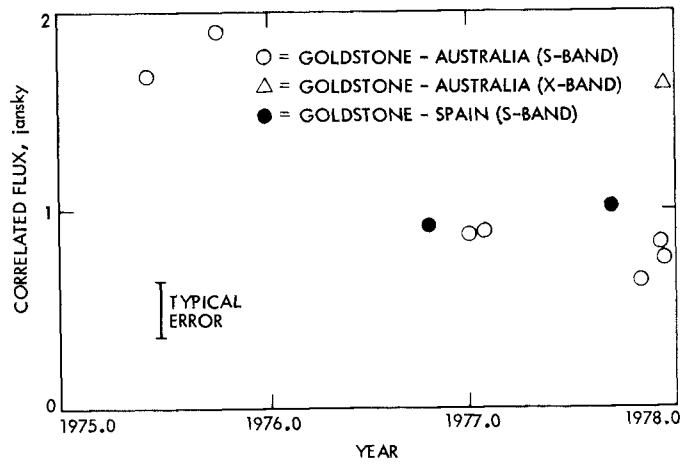

Fig. 4. OJ287 correlated flux history

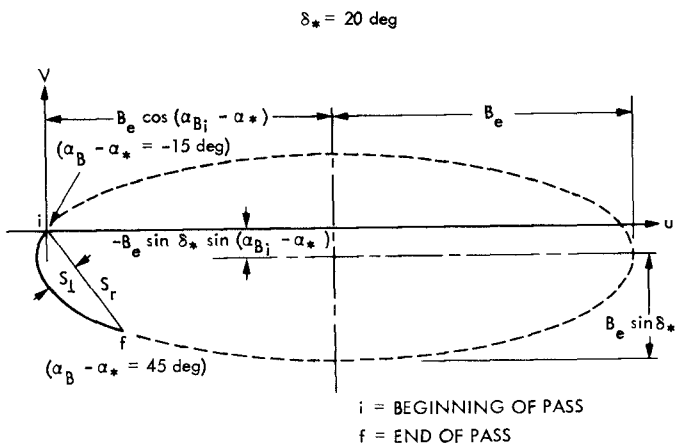

Fig. 5. Information content ellipse of fringe phase Δ VLBI

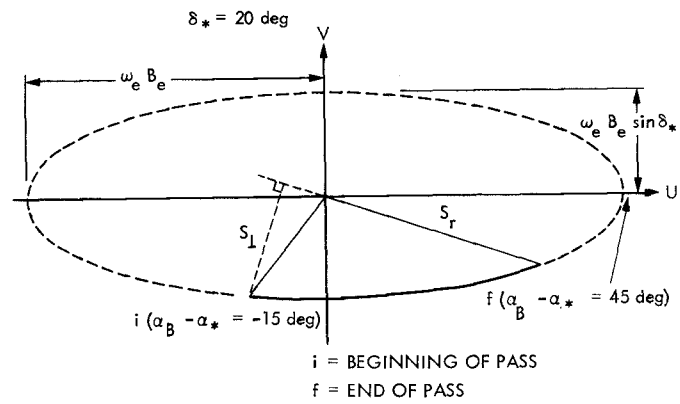

Fig. 6. Information content ellipse of fringe-phase-rate Δ VLBI

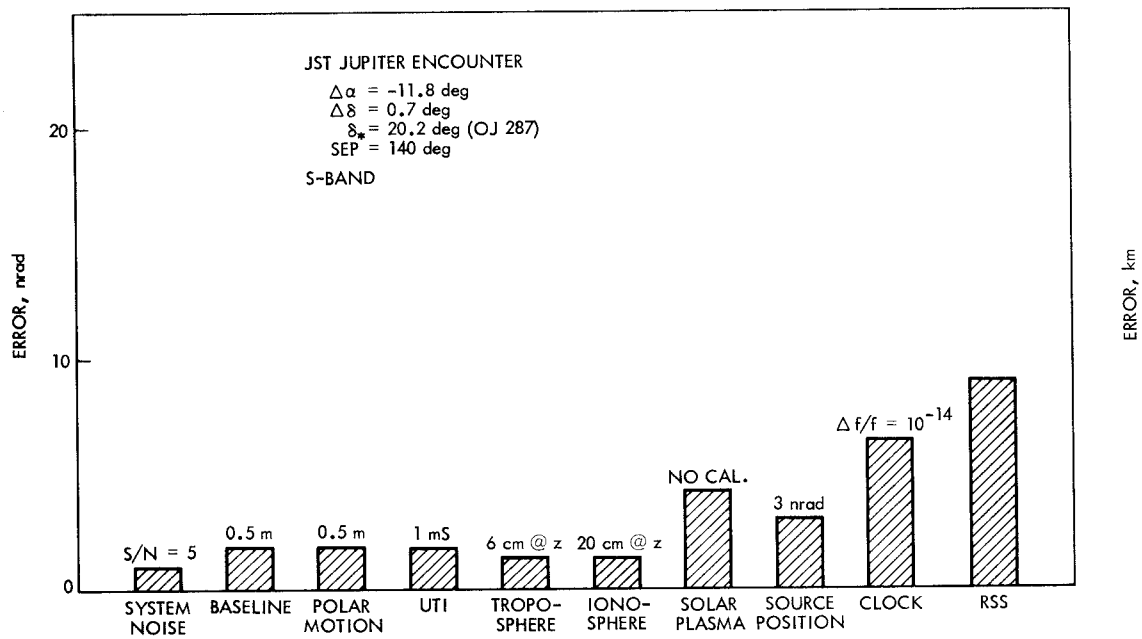

Fig. 7. Δ VLBI error sources during JST Jupiter encounter

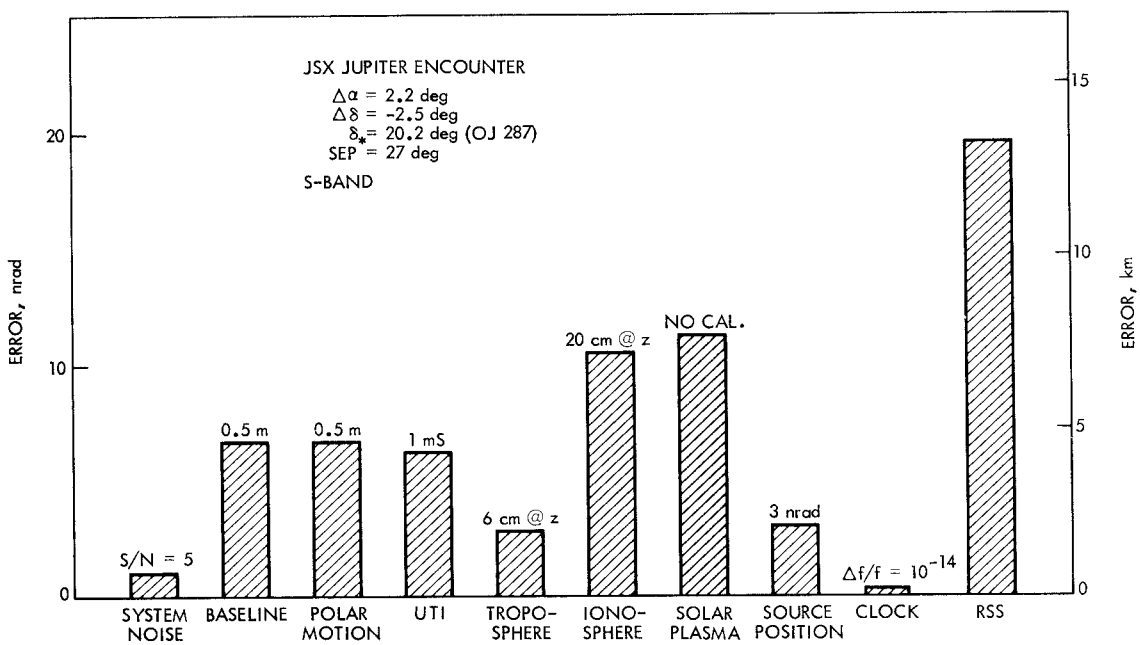

Fig. 8. Δ VLBI error sources during JSX Jupiter encounter

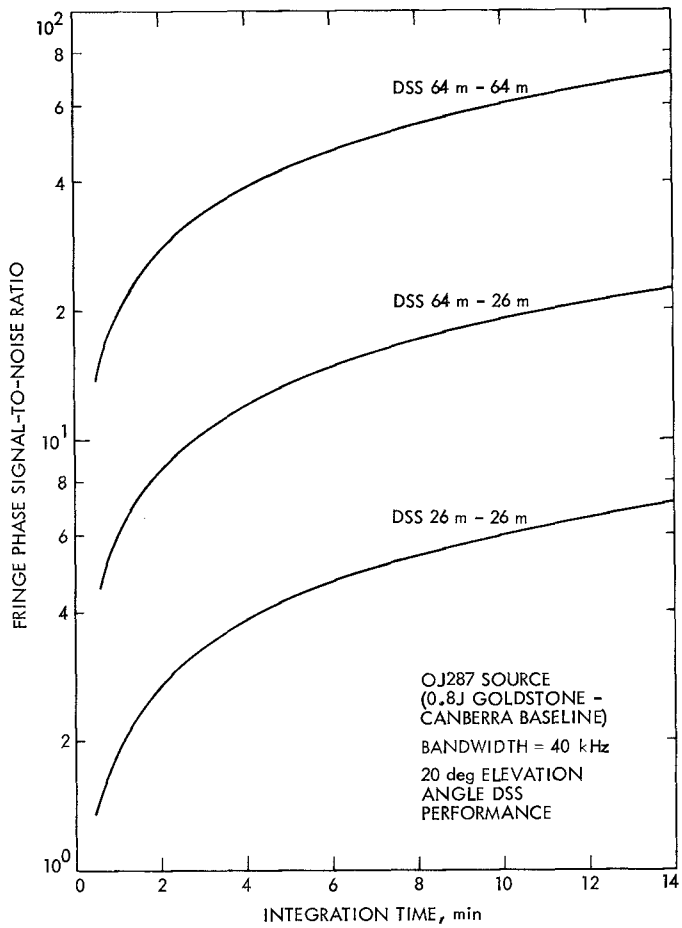

Fig. 9. S-band narrow-band EGRS Δ VLBI performance OJ287 source (0.8J Goldstone-Canberra baseline)

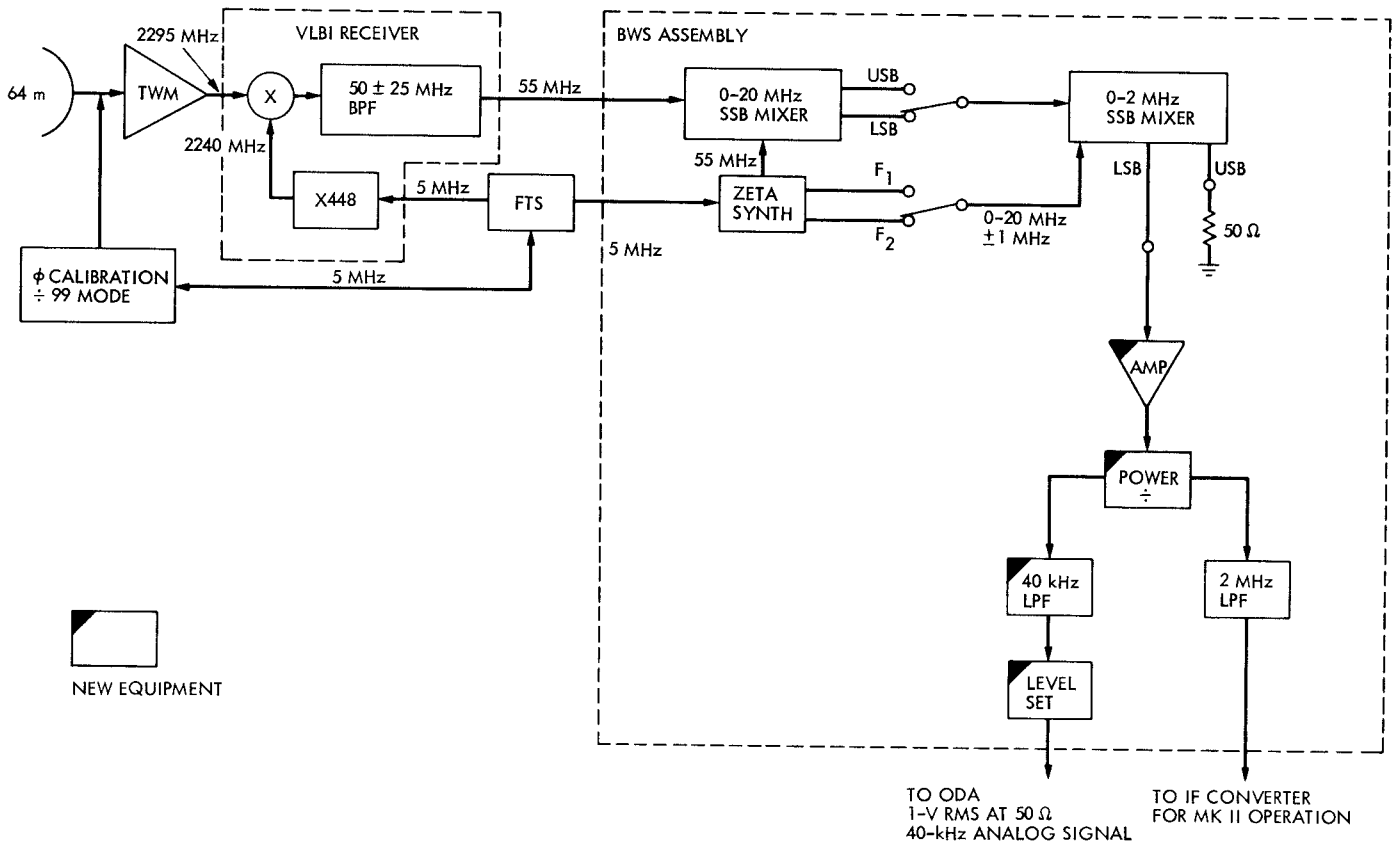

Fig. 10. DSS 14 S-band near real-time VLBI data acquisition system for Voyager demonstration

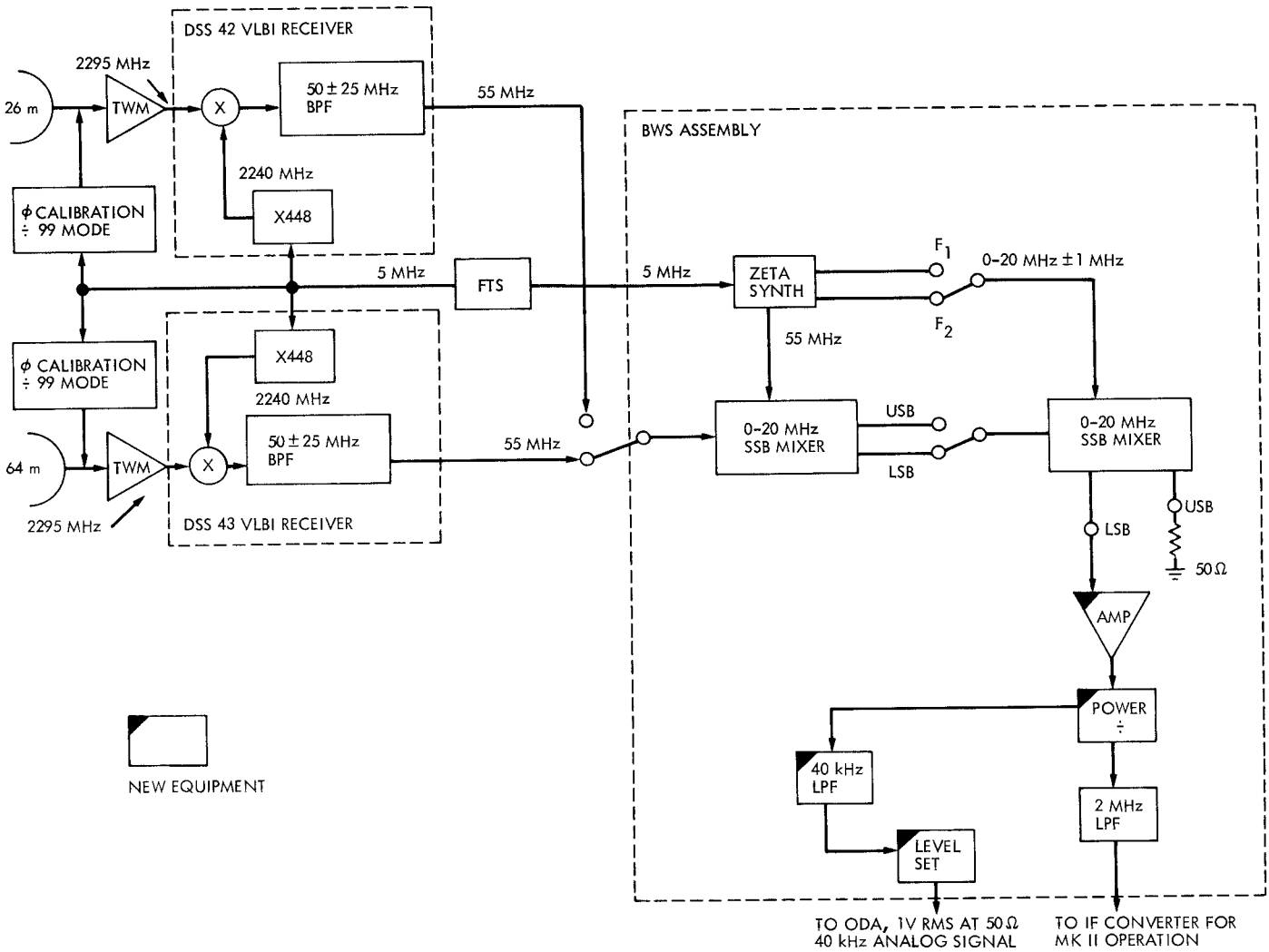

Fig. 11. Conjoint station S-band near real-time VLBI data acquisition system for Voyager demonstration

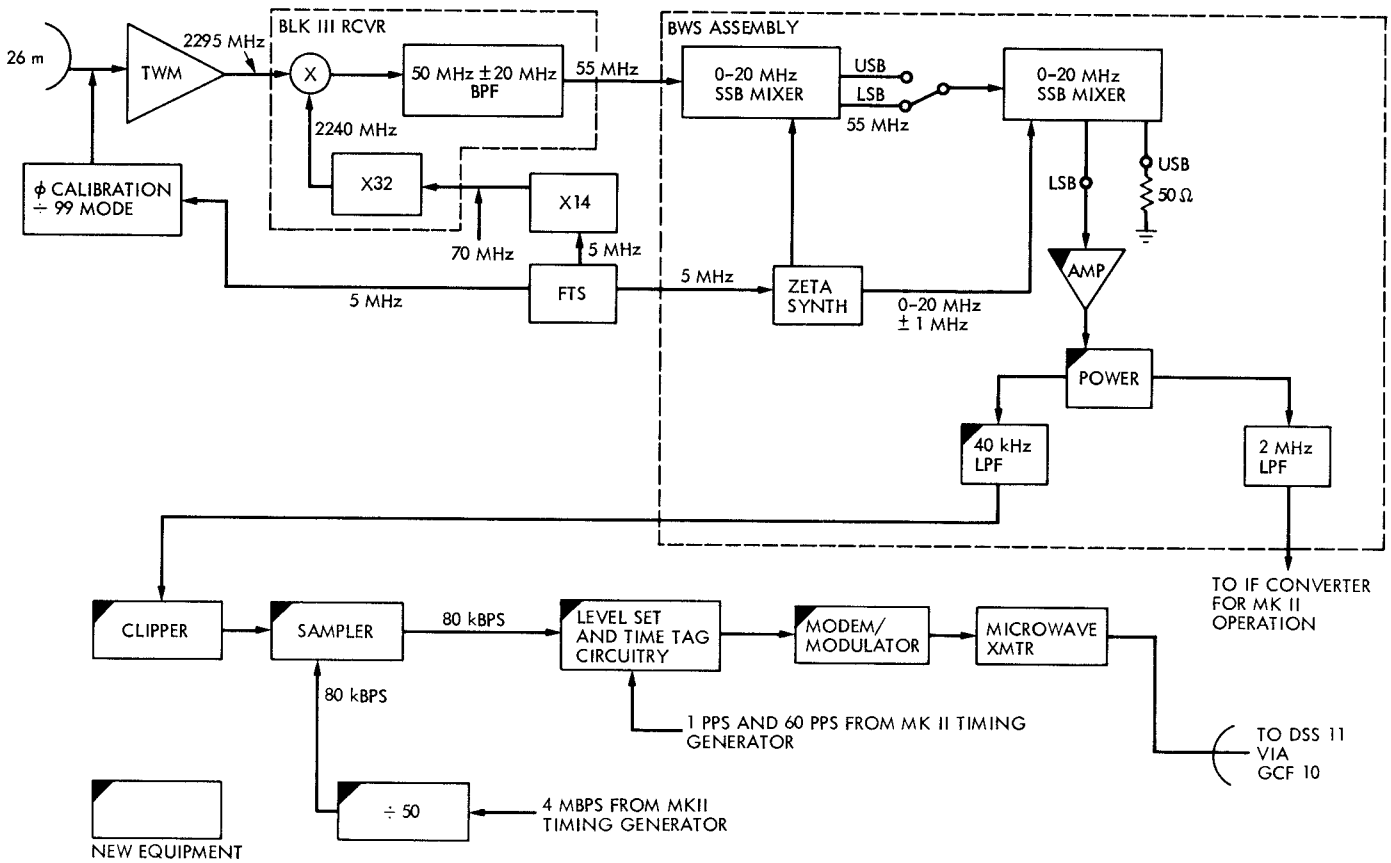

Fig. 12. DSS 13 S-band near real-time VLBI acquisition system for Voyager demonstration

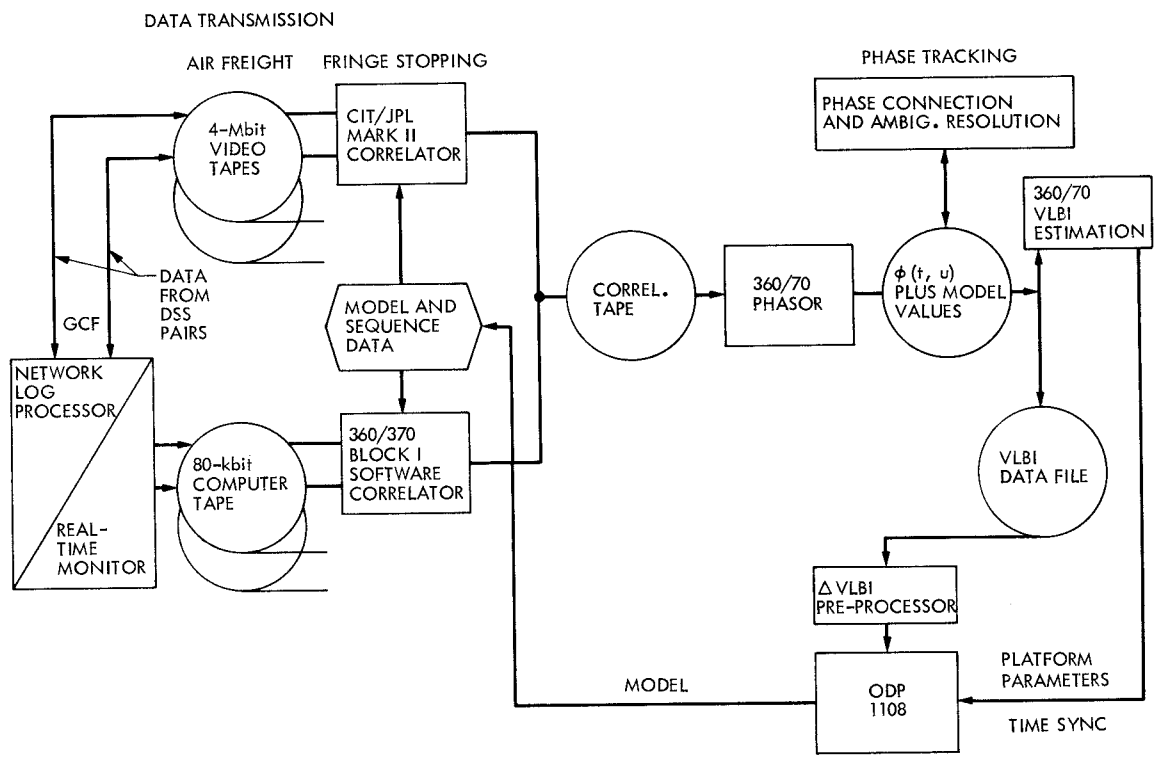

Fig. 13. VLBI navigation R & D processing system